



Huey-Wen Lin

Hadron Spectroscopy and Structure from Lattice QCD

Received: 19 April 2022 / Accepted: 25 July 2022 / Published online: 6 September 2022
© The Author(s), under exclusive licence to Springer-Verlag GmbH Austria, part of Springer Nature 2022

Abstract Lattice QCD is a theoretical tool that allows us to study the nonperturbative regime of QCD directly with full systematic control. The approach is based on regularizing QCD on a finite four-dimensional Euclidean spacetime lattice and is often studied using numerical computations of QCD correlation functions in the path-integral formalism using national-scale supercomputers. To make contact with experimental data, the numerical results are extrapolated to the continuum (with lattice spacing $a \rightarrow 0$) and infinite-volume ($L \rightarrow \infty$) limits. When the calculation is done using heavier-than-physical quark masses (to save computational time), one also has to take the $m_q \rightarrow m_q^{\text{phys}}$ limit. In the past decade, there has been significant progress in the development of efficient algorithms for the generation of ensembles of gauge-field configurations and tools for extracting relevant information from lattice-QCD correlation functions. Lattice-QCD calculations have reached a level where they not only complement, but also guide current and forthcoming experimental programs. In this lecture, we will briefly describe the methodology of lattice calculations on the topics of hadron spectroscopy and structure.

1 Lattice QCD in a Nutshell

Lattice QCD (LQCD) is an ideal theoretical tool to study the parton structure of hadrons, starting from quark and gluon degrees of freedom. Lattice QCD discretizes four-dimensional continuum QCD to allow the study of the strong-coupling regime of QCD, where perturbative approaches converge poorly, and some relevant physics may not be captured correctly. As in continuum QCD, we calculate an observable of interest through a path integral:

$$\langle 0 | O(\bar{\psi}, \psi, A) | 0 \rangle = \frac{1}{Z} \int [dA][d\bar{\psi}][d\psi] O(\bar{\psi}, \psi, A) e^{i \int d^4x \mathcal{L}_{\text{QCD}}(\bar{\psi}, \psi, A)}, \quad (1)$$

where \mathcal{L}_{QCD} is the sum of the pure-gauge and fermion Lagrangian, O is the operator that gives the correct quantum numbers for physical observable, and Z is the partition function of the spacetime integral of the QCD Lagrangian. It is straightforward to carry out this path integral numerically within a finite spacetime volume

¹ The lattice spacing is often set by matching a physical quantity, such as a hadron mass, between the calculation and experiment. For some observables where the LQCD determination is very precise, such as the strong coupling constant α_s [1], the scale-setting procedure can be the largest source of uncertainty.

H.-W. Lin (✉)
Department of Physics and Astronomy, Michigan State University, East Lansing, MI 48824, USA
E-mail: hwlin@pa.msu.edu

H.-W. Lin
Department of Computational Mathematics, Science and Engineering, Michigan State University, East Lansing, MI 48824, USA

and under an ultraviolet cutoff (the lattice spacing a). For observables that have a well-defined operator in the Euclidean path integral for numerical integration, we can find their values in continuum QCD by taking the limits lattice spacing $a \rightarrow 0$,¹ spatial size $L \rightarrow \infty$ and quark mass $m_q \rightarrow m_q^{\text{phys}}$.

In order to make predictions using QCD on the lattice, we calculate observables corresponding to vacuum expectation values of operators O , taking the form

$$\begin{aligned} \langle O \rangle &= \frac{1}{Z} \int [dU][d\psi][d\bar{\psi}] e^{-S_F(U, \psi, \bar{\psi}) - S_G(U)} O(U, \psi, \bar{\psi}) \\ &= \frac{1}{Z} \int [dU] \det M e^{-S_G(U)} O(U) \\ &= \frac{1}{Z} \int [dU] e^{-S_{\text{eff}}(U)} O(U), \end{aligned} \quad (2)$$

where

$$Z = \int [dU][d\psi][d\bar{\psi}] e^{-S_F - S_G}, \quad (3)$$

S_G is the gauge action and $S_F = \bar{\psi} M \psi$ is the fermion action with Dirac operator M . The bilinear structure of the fermion action allows the integration over the fermion fields to be done explicitly, bringing down a factor of $\det M$. This means that the anticommuting fermion fields (impossible to simulate on a computer) are integrated out, leaving an integrand that depends only the values of the gauge fields. In the early days of lattice QCD, the computational resources were insufficient to compute the fermionic determinant; instead, the determinant was approximated by a constant. This is equivalent to removing quark loops from the Feynman diagrams of a perturbative expansion, and this technique became known as the ‘‘quenched approximation’’. Quenching retains many of the important properties of QCD, such as asymptotic freedom and confinement, and the computational cost is much cheaper. It can be useful to study large numbers of configurations or much smaller lattice spacings to provide insights before moving to calculations orders-of-magnitude more computationally costly with the up, down and strange quarks in the sea.

The discrete integral we have derived can be evaluated numerically using Monte-Carlo methods. Monte-Carlo integration uses random points within the domain of gauge configurations to approximately evaluate the integral. The ‘‘importance sampling’’ technique is introduced to perform this task more efficiently: instead of choosing points from a uniform distribution, they are chosen from a distribution proportional to the Boltzmann factor $e^{-S_{\text{eff}}(U)}$, which concentrates the points where the function being integrated is large.

Using this method, we accumulate an ensemble of gauge-field configurations (see the right-hand side of Fig. 1 for an illustration), generated using a Markov-chain technique. Based on the current state of the gauge configuration, a new configuration is selected. A transition probability $P([U'] \leftarrow [U])$ is determined based solely on this new configuration and the current one. The new configuration is added to the ensemble or rejected, according to the resulting probability. If the ‘‘detailed balance’’ condition

$$P([U'] \leftarrow [U]) e^{-S_{\text{eff}}(U)} = P([U] \leftarrow [U']) e^{-S_{\text{eff}}(U')} \quad (4)$$

is satisfied by this update procedure, then the canonical ensemble is a fixed point of the transition probability matrix. Under this condition, repeated updating steps will bring the gauge-field distribution to the canonical ensemble. These calculations require high-performance supercomputer centers with software developed by and shared among the community. The right-hand side of Fig. 1 shows an example of commonly used software from the US lattice community and their dependencies. Once the proper QCD vacuum is obtained, one can move on to calculate QCD observables, such as spectroscopy and structure of hadrons.

2 Hadron Spectroscopy on the Lattice

Some of the primary observables we study on the lattice are two-point correlation functions. A particle of interest is created by an operator carrying the appropriate quantum numbers. For example, meson states can be created with local bilinear operators as shown in Table 1. Baryons may be constructed in the same way;

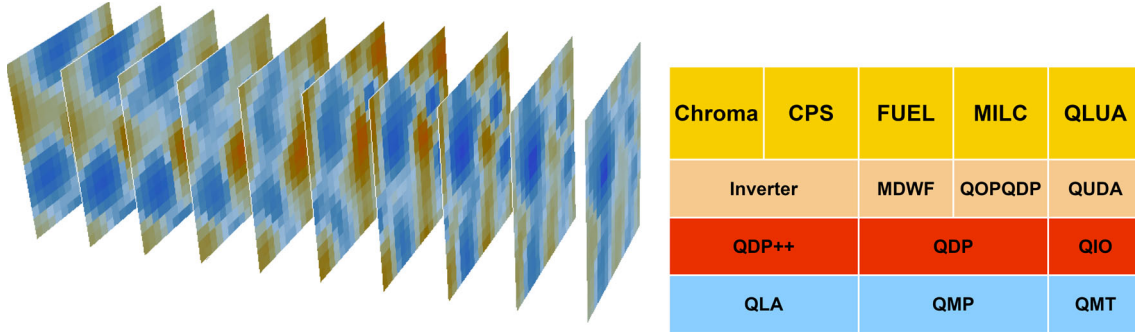


Fig. 1 (left) Illustration of an example topological QCD vacuum of the $N_f = 2 + 1 + 1$ gauge field configurations (generated by MILC collaboration). (right) The SciDAC Layers showing the modular software architecture; taken from USQCD software website, <https://usqcd-software.github.io>

Table 1 Meson states created by local operators of the form $\bar{\psi} \Gamma \psi$, labeled in spectroscopic notation

Γ	$2S+1 L_J$	J^{PC}	States
γ_5	$^1 S_0$	0^{-+}	π, η_c
γ_i	$^3 S_1$	1^{--}	$\rho, J/\Psi$
$\gamma_i \gamma_j$	$^1 P_1$	1^{+-}	b_1, h_c
1	$^3 P_0$	0^{++}	a_0, χ_{c0}
$\gamma_5 \gamma_i$	$^3 P_1$	1^{++}	a_1, χ_{c1}

for example, for nucleon spin-1/2, we can write down 3 local-site (that is all 3 quarks resides within the same lattice point) operators:

$$\begin{aligned}
 \chi_N^{(1)}(x) &= \epsilon^{abc} (u^{T,a}(x) C \gamma_5 d^b(x)) u^c(x) \\
 \chi_N^{(2)}(x) &= \epsilon^{abc} (u^{T,a}(x) C d^b(x)) \gamma_5 u^c(x) \\
 \chi_N^{(3)}(x) &= \epsilon^{abc} (u^{T,a}(x) C \gamma_5 \gamma_4 d^b(x)) u^c(x)
 \end{aligned} \tag{5}$$

More complicated hadrons (such as pentaquarks) and multiparticle states simply increase the number of quarks and antiquarks involved.

For a meson created at a specific spacetime $y = (\mathbf{y}, 0)$ (point source) and annihilated at $x = (\mathbf{x}, t)$ (point sink), the corresponding Euclidean two-point function is

$$C^{(2)}(x, y) = \langle \bar{O}(x) O(y) \rangle = \frac{1}{Z} \int [dU][d\psi][d\bar{\psi}] e^{-S_{\text{eff}}(U, \psi, \bar{\psi})} (\bar{\psi}(x) \Gamma \psi(x)) (\bar{\psi}(y) \Gamma \psi(y)). \tag{6}$$

What if we want to get to even higher excited states with LQCD? Unfortunately, in Euclidean space, excited-state contributions to correlation functions decay faster than the ground state, since each state contributes to the two-point correlator proportional to e^{-Et} , where E is the energy of the state and t is Euclidean time. Therefore, at large times, the signals for excited states are swamped by the signals for lower-energy states. One way resolve this issue is to improve resolution in the temporal direction. An anisotropic lattice where the temporal lattice spacing is finer than spatial spacings can provide better resolution while avoiding the increase in computational cost associated with a similar reduction of all spacings.

One also needs large basis of independent operators that allow the maximal overlap with higher-spin operators. The use of cubic-group irrep operators or operators constructed according to continuum symmetries is needed to expand the reach of the lattice calculation. The variational method becomes quite reliable when allowed to consider up to the 8th excited state.

Another important tool for extracting highly excited states is the variational method [2,3], which uses a matrix of different source and sink operators to project more exactly onto the eigenstates of the Hamiltonian and make the analysis more reliable. To use the method effectively, we need a large number of independent operators that overlap well with excited states with desired quantum numbers and linearly independent of with each other. Unfortunately, the single-site baryon operators of form given in Eq. 5 can only give us 3 different

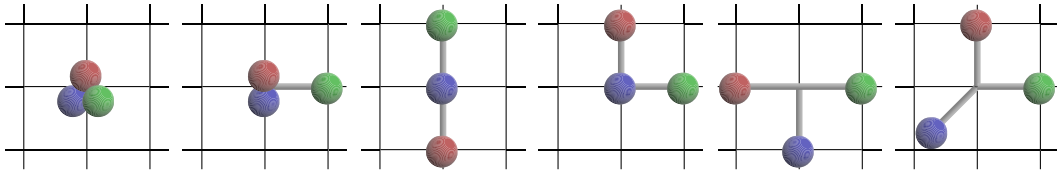


Fig. 2 The orientations of 3 quarks within a single baryon. The rightmost one involves all 3 spatial axes. The quark displacements shown above use only quarks separated from the central core by one unit; however, larger displacements can be used to improve overlap with higher orbitally excited states

operators. We need to expand our consideration to a bigger operator space to extract highly excited states reliably.

The Hadron Spectrum Collaboration (HSC) has been investigating interpolating operators projected into irreducible representations (irreps) of the cubic group [4,5] in order to better calculate two-point correlators for nucleon spectroscopy. First, we construct various gauge-invariant baryonic operators by displacing (with appropriate gauge parallel transport) the component quarks in spatial directions as shown in Fig. 2 and compose them with the appropriate flavor structure, isospin and strangeness. This large basis of operators does not respect rotational symmetry nor the subgroup of rotations that are also respected by the lattice. We apply group-theoretical projections such that operators will transform according to an irreducible representation under lattice rotations and reflections. Since the action of the lattice theory respects these symmetries, the representation of a state is conserved as it propagates through the lattice gauge field; operators belonging to different representations will not mix even as they move from source to sink. Using such a design for the operators, we can create large correlator matrices, and the technique can be extended to meson and multi-hadron computations.

In the cubic group O_h , for baryons, there are four two-dimensional irreps $G_{1g}, G_{1u}, G_{2g}, G_{2u}$ and two four-dimensional irreps H_g and H_u . (The subscripts “g” and “u” indicate positive and negative parity, respectively.) Each lattice irrep contains parts of many continuum states. The G_1 irrep contains $J \in \{\frac{1}{2}, \frac{7}{2}, \frac{9}{2}, \frac{11}{2}, \dots\}$ states, the H irrep contains $J \in \{\frac{3}{2}, \frac{5}{2}, \frac{7}{2}, \frac{9}{2}, \dots\}$ states, and the G_2 irrep contains $J \in \{\frac{5}{2}, \frac{7}{2}, \frac{11}{2}, \dots\}$ states. The continuum-limit spins J of lattice states must be deduced by examining patterns of degeneracy between the different O_h irreps. For example, G_1 will be dominated by spin-1/2 baryons with some contribution from highly excited spin-7/2 states. The H irrep will contain the spin-3/2 baryons (such as the ground-state Delta), but it will also contain many closely spaced states from all higher spins. G_2 will contain spin-5/2 and 7/2 states and serves as an important check of these spins in the H and G_1 channels. Using these operators, we construct an $r \times r$ correlator matrix and extract individual excited-state energies by applying the variational method, as described above. More details on the baryon correlation functions evaluated using the displaced-quark operators are described in Refs. [4,5]. Demonstrations of how these operators work using purely gluonic vacuum with light valence quarks for nucleon and delta spectroscopy are reported in Refs. [6–8].

One drawback of calculations using these cubic-group operators is that they require multiple orientations in order to maximally overlap with a wide range of quantum numbers, and generating so many correlators is quite expensive. Furthermore, as we go to lighter and lighter pion masses, there will be increasingly many decay modes open, even for the lowest energy at a specific quantum number. We need to extend the matrix to include multiple-particle operators (so that we can further understand the nature of the “resonance” in LQCD calculation) and “disconnected” operators. Further, we need to achieve better precision for each state to distinguish among them.

An improved way to calculate timeslice-to-all propagators, “distillation”, has been proposed in Ref. [9]. The method is useful for creating complex operators, such as those used in the variational method, since it reduces the amount of time needed for contractions and allows the structure of the operators to be decided after performing the Dirac inversions. Rather than using pure noise in its estimators, distillation uses sources derived from the eigenvectors of the gauge-Laplacian, giving better coverage of relevant degrees of freedom. Increasing the number of sources in this scheme improves statistics faster than $1/\sqrt{N}$. Distillation can be combined with stochastic methods, which might be desirable if the number of sources needed to cover the volume becomes too large.

The distillation operator on time-slice t can be written as

$$\square(t) = V(t)V^\dagger(t) \rightarrow \square_{xy}(t) = \sum_{k=1}^N v_x^{(k)}(t)v_y^{(k)\dagger}(t), \quad (7)$$

where the $V(t)$ is a matrix containing the first through k th eigenvectors of the lattice spatial Laplacian. The baryon operators involve displacements (\mathcal{D}_i) as well as coefficients ($S_{\alpha_1\alpha_2\alpha_3}$) in spin space:

$$\chi_B(t) = \epsilon^{abc} S_{\alpha_1\alpha_2\alpha_3} (\mathcal{D}_1 \square d)_{\alpha_1}^a (\mathcal{D}_2 \square u)_{\alpha_2}^b (\mathcal{D}_3 \square u)_{\alpha_3}^c(t), \quad (8)$$

where the color indices of the quark fields acted upon by the displacement operators are contracted with the antisymmetric tensor, and sum over spin indices. Then one can construct the two-point correlator; for example, in the case of proton,

$$\begin{aligned} C_B^{(2)}[\tau_d, \tau_u, \tau_u](t', t) &= \Phi^{(i,j,k)}(t') \tau_d^{(i,\bar{i})}(t', t) \tau_u^{(j,\bar{j})}(t', t) \tau_u^{(k,\bar{k})}(t', t) \Phi^{(\bar{i},\bar{j},\bar{k})^*}(t) \\ &\quad - \Phi^{(i,j,k)}(t') \tau_d^{(i,\bar{i})}(t', t) \tau_u^{(j,\bar{k})}(t', t) \tau_u^{(k,\bar{j})}(t', t) \Phi^{(\bar{i},\bar{j},\bar{k})^*}(t), \end{aligned} \quad (9)$$

where the ‘‘baryon elemental’’

$$\Phi_{\alpha_1\alpha_2\alpha_3}^{(i,j,k)}(t) = \epsilon^{abc} \left(\mathcal{D}_1 v^{(i)} \right)^a \left(\mathcal{D}_2 v^{(j)} \right)^b \left(\mathcal{D}_3 v^{(k)} \right)^c(t) S_{\alpha_1\alpha_2\alpha_3} \quad (10)$$

can be used for all flavors of baryon and quark masses with the same displacements on the same ensemble, and the ‘‘perambulator’’

$$\tau_{\alpha\beta}(t', t) = V^\dagger(t') M_{\alpha\beta}^{-1}(t', t) V(t) \quad (11)$$

can be reused for different baryon (and meson) operators after a single inversion of the M matrix. There is a large factor of computational power saved by ‘‘factorizing’’ correlators in terms of elementals and perambulators, and the same elementals and perambulators can be used to contract various different correlators.

A variations of the distillation Ref. [10–12], called stochastic LapH method, has been developed to improve the efficiency when work on even larger volumes; a demonstration on the excited-meson and -baryon, and pion-pion scattering phase shift are shown in these references.

A procedure called ‘‘pruning’’ can be used to reduce the number of operators when the size of a correlator matrix begins to get out of hand. A practical procedure is to calculate the correlators with the same source and sink operator (i.e., the diagonal elements of the full correlator matrix) and sort them according to some metric of their ‘‘individuality’’. One way to systematically prune is to take the matrix of inner products of the effective masses of each correlator across all time slices and sort them from there. This measures a sense in which the effective masses of different correlators have the same shape, implying that they also have the same excited-state content, and takes advantage of the black-box nature of the effective mass to eliminate ambiguity.

As lattice calculations approach physical pion mass, increasingly many excited hadrons can decay to more than one final state, as observed in experiments. This makes it desirable to compute the energy-dependence of coupled-channel scattering amplitudes, which connect to the discrete spectrum of eigenstates of quantum field theory in a finite volume, computed in LQCD [13–31]. This is very active area of research, where new methods have been developed in recent years. Most study has been focused on meson cases. The simplest case is elastic scattering, where in a limited energy region, only one hadron–hadron channel is kinematically open. Resonances appearing in elastic scattering include the ρ and the σ in $\pi\pi$ scattering, the K^* in πK , and the Δ in πN , all of which have been considered in LQCD [32–48]. The scattering amplitude can be described by a single real energy-dependent parameter, the phase shift, which has a characteristic rise through 90° if a narrow resonance is present. Lattice calculations are made to achieve a robust determination of the discrete spectrum of eigenstates via several lattice volumes; one can then simply map each discrete energy level in a finite volume to a value of the elastic scattering phase shift at that energy (neglecting higher partial waves) [3, 13].

Going beyond the simplest case of elastic scattering, resonances will appear in the coupled-channel S -matrix, and there can no longer be a one-to-one mapping of any given energy level into the multiple unknowns of a coupled-channel scattering matrix at that energy [13]. Refs. [38, 49–53] suggest studying multiple choices of parametrization forms to fit the energy-dependence of coupled-channel amplitudes, and to use very many

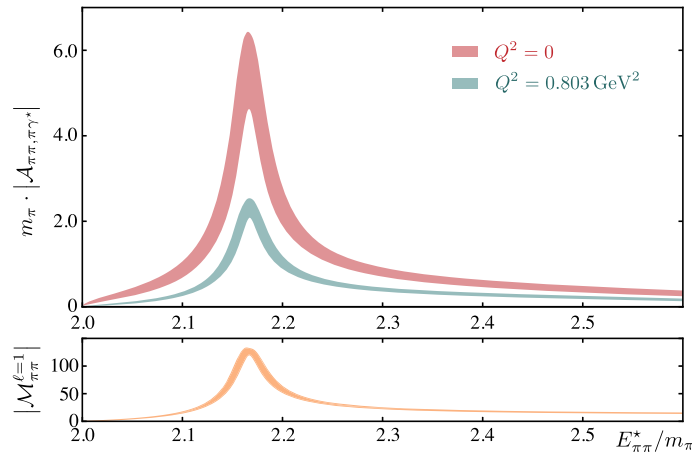


Fig. 3 Amplitude for the process $\pi\gamma^* \rightarrow \pi\pi$ in P -wave computed in lattice QCD at $M_\pi \approx 400$ MeV [54,55]. The figure shows two values of the photon virtuality Q^2 and the corresponding amplitude for $\pi\pi \rightarrow \pi\pi$, which indicates that the ρ resonance is contributing to both processes

discrete energy levels in multiple volumes and/or moving frames to constrain the free parameters. Refs. [54,55] report the first explicit calculation of three-point vector current correlation functions corresponding to the process $\gamma^*\pi \rightarrow \pi\pi$ with $J^P = 1^-$ at $M_\pi \approx 400$ MeV, as shown in Fig. 3. The effect of the ρ resonance in the electromagnetic transition amplitude is observed. The dependence on the virtuality of current can be used to determine the transition form factor of the unstable ρ resonance. This is a very active research area in the lattice QCD; we refer interested readers to these selected reviews [56–59].

3 Hadron Structure on the Lattice

Lattice QCD is an ideal theoretical tool to study the parton structure of hadrons, starting from quark and gluon degrees of freedom. To study the structure of a hadron, one also starts with a QCD vacuum, creating a hadron at a “source” location using choices of the operator described above and inserting a “probe” (can be a local or nonlocal operator) before annihilating the hadron at the end “sink” location. One can have the initial and final hadron at rest (preferred setup for typical charges and leading-moment calculations), at different initial and final momenta (to obtain form factors), or in Breit frame with equal-time nonlocal spatial Wilson-line for Bjorken- x dependence of the generalized parton distribution (GPDs) (see an example of the lattice setup in the left-hand side of Fig. 4).

The progress of lattice hadron calculations has long been limited by computational resources, but recent advances in both algorithms and a worldwide investment in pursuing exascale computing has led to exciting progress in LQCD calculations. Take the nucleon tensor charge, for example. Experimentally, one gets the tensor charges by taking the zeroth moment of the transversity distribution; however, the transversity distribution is poorly known and such a determination is not very accurate. On the lattice side, there are a number of calculations of isovector nucleon calculation of g_T [60–68]; some of them are done with more than one ensemble at physical pion mass with high-statistics calculations (about 100k measurements) and some with multiple lattice spacings and volumes to control lattice artifacts. Such programs would have been impossible 5 years ago. As a result, the lattice-QCD tensor-charge calculation has the most precise determination of this quantity, which can then be used to constrain the transversity distribution and make predictions for upcoming experiments [69]. Reference [69] uses the lattice-averaged isovector g_T to constrain the global-analysis fits of SIDIS charged-pion-production data from proton and deuteron targets, including their x , z and P_\perp dependence, with a total of 176 data points collected from measurements at HERMES and COMPASS. This gives in principle eight linear combinations of transversity TMD PDFs and Collins TMD FFs for different quark flavors, from which we attempt to extract the u and d transversity PDFs and the unflavored Collins FFs, together with their respective transverse-momentum widths, as shown on the right-hand side of Fig. 4. Without the lattice constraints, the distribution is consistent with zero within 2 sigma; with the constraint from the lattice tensor charge, the results are greatly improved and can make predictions at large- x transversity for both up and down quarks for upcoming measurements at Jefferson Lab and other facilities. Note that the lattice g_T only provides

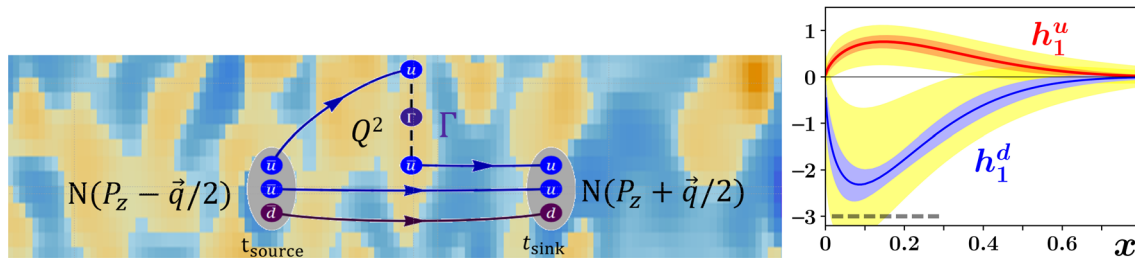


Fig. 4 (left) Illustration of an example matrix-element calculation for a generalized parton distribution, depicted on top of the lattice QCD vacuum. (right) LQCD g_T constraint on transversity PDFs $h_1^{u,d}$ for SIDIS with (red/blue) and without (yellow) lattice inputs at $Q^2 = 2 \text{ GeV}^2$, compared with the SIDIS-only fit uncertainties (yellow bands) [69]

information on the integrated difference between the up and down h_1 function; by itself it does not tell us any information about the shape of the transversity distribution. Only when one combines both lattice and experimental data does such a prediction become possible. One can imagine that many of the quantities less known from experiments can greatly benefit from lattice-QCD predictions and constraints. Due to the page limit, we refer interested readers to read these recent reviews for more details on lattice moments [70, 71]. For the rest of the lecture, we will focus on selected results with the new methods that enable lattice calculations to determine the Bjorken- x distribution of hadrons.

3.1 Nucleon PDFs

There has been rapid progress calculating the Bjorken- x dependence of PDFs on the lattice since the proposal of large-momentum effective theory (LaMET, also called the “quasi-PDF” method) [72, 73]. LaMET relates equal-time spatial correlators, whose Fourier transforms (FTs) are called quasi-PDFs, to PDFs in the limit of infinite hadron momentum. For large but finite momenta accessible on a realistic lattice, LaMET relates quasi-PDFs to physical ones through a factorization theorem, the proof of which was developed in Refs. [74–76]. Since the first lattice x -dependent PDF calculation [77], much progress has been made and calculations done. For recent reviews, see Refs. [70, 78–80]. Here, we highlight a few calculations at physical pion mass.

The most studied x -dependent structures are the nucleon unpolarized isovector parton distribution functions (PDFs) where the gluon and quark “disconnected” loops are cancelled due to the isospin symmetry of the up and down quark masses in most lattice hadron-structure calculations. The right-hand side of Fig. 5 shows a state-of-the-art lattice calculation of the nucleon isovector unpolarized PDFs calculated. Most of the calculated are performed at one single ensemble (see Fig. 7 in Ref. [80]) excepting the results from MSULat group [81]. The lattice results are calculated using ensembles with multiple sea pion masses with the lightest one around 135 MeV, three lattice spacings $a \in [0.06, 0.12]$ fm, and multiple volumes with $M_\pi L$ ranging 3.3–5.5. A simultaneous chiral-continuum extrapolation is performed on the RI/MOM-renormalized nucleon matrix elements with various Wilson-link displacements to obtain the physical-continuum matrix elements. Then apply one-loop perturbative matching to the quasi-PDFs to obtain the lightcone PDFs, and compare the LQCD results with a selection of global-fit PDFs. The lattice nucleon isovector PDFs (with statistical and estimated systematic errors shown as inner/outer band) has nice agreement with those obtained from global fits, CT18NNLO [82], NNPDF3.1NNLO [83], ABP16 [84], and CJ15 [85]. The errors increase toward the smaller- x region for both lattice and global fitted PDFs, but overall, they agree within two standard deviations.

The middle and right panels of Fig. 5 show a summary of the lattice nucleon isovector helicity and transversity PDFs at the physical pion mass, respectively, obtained from Refs. [61, 86–88]. The helicity lattice results are compared to two phenomenological fits, NNPDFpol1.1 [89] and JAM17 [90], exhibiting nice agreement. The lattice results for the transversity PDFs has better precision than the global analysis by PV18 and LMPSS17 [69]. Note that none of these current polarized lattice calculations have taken the continuum limit ($a \rightarrow 0$) and have remaining lattice artifacts (such as finite-volume effects); disagreement among the lattice results in the obtained distributions is not unexpected. Further studies of the systematic uncertainties, including multiple lattice spacings and volumes, from each collaboration will be needed.

The first lattice-QCD calculations of the strange and charm parton distributions using LaMET approach were also reported in Ref. [96]. The study found that the renormalized real matrix elements are zero within the statistical errors for both strange and charm, supporting the strange-antistrange and charm-anticharm symmetry

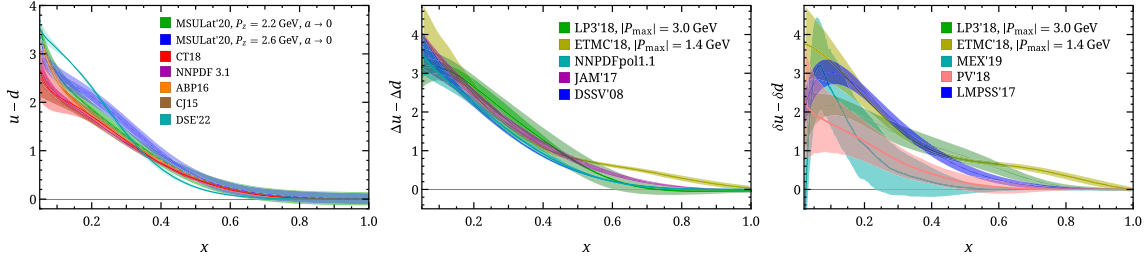


Fig. 5 (left) The first lattice calculation of continuum-physical limit nucleon isovector unpolarized PDFs [80] is compared with global fits from Refs. [82–85] and DSE’22 [91] Summary of the lattice calculation of isovector helicity (middle) and transversity (right) with LP3 and ETMC isovector quark taken from LP318 [61,88], ETMC18 [87,92], and global fits from NNPDFpol1.1 [89], JAM17 [90], DSSV08 [93] (helicity), MEX19 [94], PV18 [95], LMPSS17 [69] (transversity)

assumptions commonly adopted by most global PDF analyses. The imaginary matrix elements are proportional to the sum of the quark and antiquark distribution, and we clearly see that the strange contribution is about a factor of 5 or larger than the charm ones. They are consistently smaller than those from CT18 and NNPDF3.1, possibly due to the missing contributions from the mixing with gluon matrix elements in the renormalization. Higher statistics will be needed to better constrain the quark-antiquark asymmetry.

3.2 Meson PDFs

The first lattice-QCD calculation of the pion and kaon valence-quark distribution functions was reported in Ref. [97,98]. The latest calculation is performed with multiple pion masses with the lightest one around 220 MeV, two lattice spacings $a = 0.06$ and 0.12 fm, $(M_\pi)_{\min} L \approx 5.5$, and high statistics ranging from 11,600 to 61,312 measurements. We perform chiral-continuum extrapolation to obtain the renormalized matrix elements at physical pion mass, using a simple ansatz to combine the data from 220, 310 and 690 MeV: $h_i^R(P_z, z, M_\pi) = c_{0,i} + c_{1,i} M_\pi^2 + c_a a^2$ with $i = K, \pi$. Mixed actions, with light and strange quark masses tuned to reproduce the lightest sea light and strange pseudoscalar meson masses, can suffer from additional systematics at $O(a^2)$; such artifacts are accounted for by the c_a coefficient. We find all the c_a to be consistent with zero.

Figure 6 shows the final results for the pion valence distribution at physical pion mass ($u_v^{\pi^+}$) multiplied by Bjorken- x as a function of x . The inner bands indicate the statistical errors while the outer bands account for systematic errors from parametrization choices in the fits, the dependence on the maximum available Wilson-line displacement, etc. We evolve the LQCD results to a scale of 27 GeV^2 using the NNLO DGLAP equations from the higher-order perturbative parton evolution toolkit (HOPPET) to compare with other results. The LQCD result approaches $x = 1$ as $(1-x)^{1.01}$ and is consistent with the original analysis of the FNAL-E615 experiment data. On the other hand, there is tension with the $x > 0.6$ distribution from the re-analysis of the FNAL-E615 experiment data using next-to-leading-logarithmic threshold resummation effects in the calculation of the Drell–Yan cross section (labeled as “ASV’10”), which agrees better with the distribution from Dyson–Schwinger equations (DSE) [99] and earlier estimate of the parton limit of QCD [100,101]; all prefer the form $(1-x)^2$ as $x \rightarrow 1$. An independent lattice study of the pion valence-quark distribution [102], also extrapolated to physical pion mass, using the “lattice cross sections” (LCSs), reported similar results to ours.²

The middle of the Fig. 6 shows the ratios of the light-quark distribution in the kaon to the one in the pion ($u_v^{K^+}/u_v^{\pi^+}$). When comparing the LQCD result with the experimental determination of the valence quark distribution via the Drell–Yan process by NA3 Collaboration in 1982, good agreement is found between the LQCD results and the data. The LQCD result approaches 0.4 as $x \rightarrow 1$ and agrees nicely with other analyses, such as constituent quark model, the DSE approach (“DSE’11” [104]), and basis light-front quantization with color-singlet Nambu–Jona-Lasinio interactions (“BLFQ-NJL’19” [105]). The LQCD prediction for $x s_v^K$ is also shown in Fig. 6 with the lowest three moments of s_v^K being $0.261(8)_{\text{stat}}(8)_{\text{syst}}$, $0.120(7)_{\text{stat}}(9)_{\text{syst}}$, $0.069(6)_{\text{stat}}(8)_{\text{syst}}$, respectively; the moment results are within the ranges of the QCD-model estimates from

² Note that there are other lattice non-physical pion mass results which reach different conclusion: For example, another work by HadStruc collaboration using $2 + 1$ -flavor QCD using the isotropic-clover fermion action at heavier than physical pion mass 416-MeV using pseudo-PDF method shows results found $(1-x)^{1.93}$ [103].

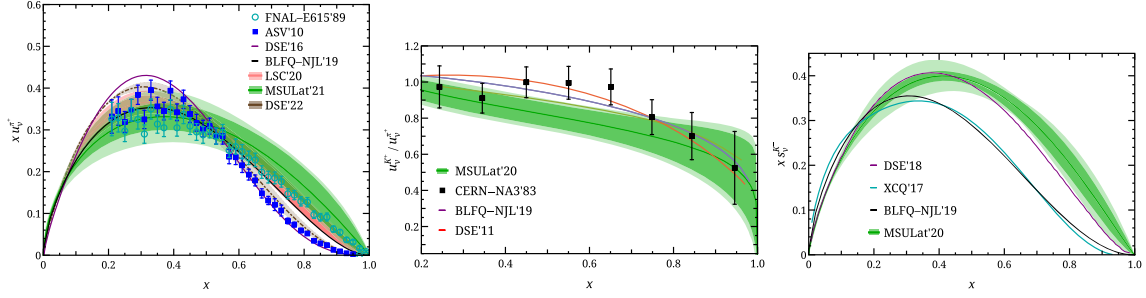


Fig. 6 Results on the valence-quark distribution of the pion (left), the ratio of the light-quark valence distribution of kaon to that of pion (middle) and $xS_V^K(x)$ as a function of x (right) at a scale of 27 GeV^2 , both labeled “MSULat’20”, along with results from relevant experiments and other calculations [98] and recent DSE’20 results [91]. The inner bands indicate statistical errors with the full range of zP_z data while outer bands includes errors from using different data choices and fit forms

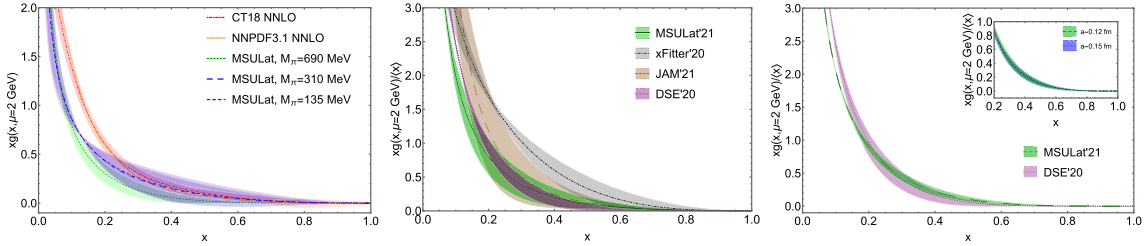


Fig. 7 The unpolarized gluon PDF, obtained from the fit to the lattice data at pion masses $M_\pi = 135$ (extrapolated), 310 and 690 MeV compared with the NNLO CT18 and NNPDF3.1 gluon PDFs. The $x > 0.3$ PDF results are consistent with the NNLO CT18 and NNPDF3.1 unpolarized gluon PDFs at $\overline{\text{MS}} \mu = 2 \text{ GeV}$ [114]. (right) The first lattice calculation of the x -dependent pion gluon PDF [106] $xg(x, \mu)/\langle x \rangle_g$ as a function of x obtained from the fit to the lattice data from the 220-MeV ensemble, along with results from JAM [116,117] and DSE [115], and xFitter [118]. The dependence on lattice spacing and pion mass is also studied in Ref. [106]. (right) The kaon gluon PDF $xg(x, \mu)/\langle x \rangle_g$ as a function of x obtained from the fit to the lattice data on ensembles with lattice spacing $a \approx \{0.12, 0.15\} \text{ fm}$ (inset plot), pion masses $M_\pi \approx 310 \text{ MeV}$ at $a \approx 0.12 \text{ fm}$, compared with the kaon gluon PDF from DSE’20 [115] at $\mu = 2 \text{ GeV}$ in the $\overline{\text{MS}}$ scheme

chiral constituent-quark model (0.24, 0.096, 0.049) and DSE [99] (0.36, 0.17, 0.092). The pion gluon PDF results can be found in Refs. [106,107].

3.3 Gluon PDFs of Nucleon and Mesons

The first exploratory study applying LQCD to gluon PDFs can be found in Ref. [108]. Since gluon quantities are much noisier than quark disconnected loops, calculations with very high statistics are necessary. The calculations were done using overlap valence fermions on gauge ensembles with $2 + 1$ flavors of domain-wall fermions at $M_\pi^{\text{sea}} = 330 \text{ MeV}$. The gluon operators were calculated for all spacetime lattice sites at high statistics: 207,872 measurements were taken of the two-point functions with valence quarks at the light sea and strange masses. The coordinate-space gluon quasi-PDF matrix element ratios are compared to the corresponding ones of the gluon PDF based on two global fits at NLO: the PDF4LHC15 combination [109] and the CT14 [110]. Up to perturbative matching and power corrections at $O(1/P_z^2)$, the lattice results are compatible with global fits within the statistical uncertainty at large z . The gluon quasi-PDFs in the pion were also studied for the first time in Ref. [108], showing features similar to those observed for the proton were revealed. Finally, there have been recent developments in improving the operators for the gluon-PDF lattice calculations [111–113], which will allow us to take the continuum limit for the gluon PDFs in future lattice calculations. Figure 7 shows the follow-up on the attempt to extract the x -dependence of the PDFs of the nucleon and pion (2 lattice spacings: 0.09 and 0.12 fm with $M_\pi \approx 220, 310$ and 690 MeV) [106,114], as well as the first kaon gluon PDF (right) at 310-MeV pion mass. The lattice pion and kaon gluon PDFs show reasonable agreement in the mid- x region with DSE work [115].

3.4 Generalized Parton Distributions (GPDs)

Generalized parton distributions provide hybrid momentum and coordinate space distributions of partons and bridge the standard nucleon structure observables: form factors and collinear PDFs. More importantly, GPDs provide information on the spin and mass structure of the nucleon. GPDs bring the energy-momentum tensor matrix elements within experimental grasp through electromagnetic scattering and can be viewed as a hybrid of parton distributions (PDFs), form factors, and distribution amplitudes. For example, the forward limit of the unpolarized and helicity GPDs lead to the $f_1(x)$ and $g_1(x)$ PDFs, respectively. Taking the integral over x at finite values of the momentum transfer results in the form factors and generalized form factors. In the case of the unpolarized GPDs, for example, one obtains the Dirac (F_1) and Pauli (F_2) form factors. Several of these limits of the GPDs have physical interpretations, for instance, the spin decomposition of the proton using Ji's sum rule [119].

GPDs parametrize the quark and gluon correlation functions involving matrix elements of operators at a lightlike separation between the parton fields [120],

$$\begin{aligned} W_{\Lambda\Lambda'}^{[\gamma^+]} &= \frac{1}{2} \int \frac{dy^-}{2\pi} e^{ik^+y^-} \langle p', \Lambda' | \bar{\psi} \left(-\frac{y}{2}\right) \gamma^+ \mathcal{U} \left(-\frac{y}{2}, \frac{y}{2}\right) \psi \left(\frac{y}{2}\right) | p, \Lambda \rangle_{y^+=y_T=0} \\ &= \frac{1}{2P^+} \langle p', \Lambda' | \gamma^+ H(x, \xi, t) + \frac{i\sigma^{+j}\Delta_j}{2M} E(x, \xi, t) | p, \Lambda \rangle \end{aligned} \quad (12)$$

$$\begin{aligned} \tilde{W}_{\Lambda\Lambda'}^{[\gamma^+\gamma_5]} &= \frac{1}{2} \int \frac{dy^-}{2\pi} e^{ik^+y^-} \langle p', \Lambda' | \bar{\psi} \left(-\frac{y}{2}\right) \gamma^+ \gamma_5 \mathcal{U} \left(-\frac{y}{2}, \frac{y}{2}\right) \psi \left(\frac{y}{2}\right) | p, \Lambda \rangle_{y^+=y_T=0} \\ &= \frac{1}{2P^+} \langle p', \Lambda' | \gamma^+ \gamma_5 \tilde{H}(x, \xi, t) + \frac{\gamma_5 \Delta^+}{2M} \tilde{E}(x, \xi, t) | p, \Lambda \rangle. \end{aligned} \quad (13)$$

Two additional kinematic variables enter their definition besides the quark lightcone longitudinal momentum fraction, $x = k^+/P^+$ (with $P = (p + p')/2$): the lightcone component of the longitudinal momentum transfer between the initial and final proton, $\xi = -\Delta^+/(2P^+) \approx x_{Bj}/(2 - x_{Bj}) > 0$ (with $\Delta = p' - p$), and the transverse component, $\Delta_T = p'_T - p_T$; the latter is taken into account through the invariant, $t = \Delta^2 = M^2\xi^2/(1 - \xi^2) - \Delta_T^2/(1 - \xi^2)$, $t < 0$). At leading (twist-two) level, four-quark chirality-conserving (chiral-even) GPDs, H , E , \tilde{H} and \tilde{E} , defined in Eqs. (12) and (13), parametrize the quark-proton correlation functions.

Information on GPDs from lattice QCD has been available via their form factors and generalized form factors, using the operator product expansion (OPE). As in PDFs, such information is limited due to the suppression of the signal as the order of the Mellin moments increases and the momentum transfer between the initial and final state increases. Significant progress has been made towards new methods to access the x - and t -dependence of GPDs ($t = -Q^2$), which is driven by the advances in PDF calculations. In lattice QCD, there are several challenges in calculating GPD using these new methods. The extraction of GPDs is more challenging than collinear PDFs, because GPDs require momentum transfer, Q^2 , between the initial (source) and final (sink) states. Another complication is that GPDs are defined in the Breit frame, in which the momentum transfer is equally distributed to the initial and final states; such a setup increases the computational cost, as separate calculations are necessary for each value of the momentum transfer.

The first lattice x -dependent GPD calculations were carried out in Ref. [121], studying the pion valence-quark GPD at zero skewness with multiple transfer momenta with pion mass $M_\pi \approx 310$ MeV. There is a reasonable agreement with traditional local-current form-factor calculations at similar pion mass, but the current uncertainties remain too large to show a clear preference among different model assumptions about the kinematic dependence of the GPD. There has also been recent progress made in lattice QCD to provide the Bjorken- x dependence of the isovector nucleon GPDs, H , E and \tilde{H} . Ref. [122] used LaMET to calculate both unpolarized and polarized nucleon isovector GPDs with largest boost momentum 1.67 GeV at pion mass $M_\pi \approx 260$ MeV with one momentum transfer. This work also presented results at nonzero skewness, with additional divergence near $x = \xi$ due to the matching. Refs. [123, 124] reported the first lattice-QCD calculations of the unpolarized and helicity nucleon GPDs with boost momentum around 2.0 GeV at physical pion mass with multiple transfer momenta, allowing study of the three-dimensional structure and impact-parameter-space distribution. Results for the moments of the integral of the H , E and \tilde{H} GPDs extracted from the lattice are within a couple sigma of previous lattice calculations using OPE operators from traditional form

factors and generalized form factors at or near the physical pion mass. Such lattice inputs can provide useful constraints to the best determination of physical quantities using both theoretical and experimental inputs.

The zero-skewness limit of GPD function is related to the Mellin moments by taking the x -moments [125, 126]:

$$\begin{aligned}
\int_{-1}^{+1} dx x^{n-1} H(x, \xi, Q^2) &= \sum_{i=0, \text{ even}}^{n-1} (-2\xi)^i A_{ni}(Q^2) + (-2\xi)^n C_{n0}(Q^2)|_{n \text{ even}}, \\
\int_{-1}^{+1} dx x^{n-1} E(x, \xi, Q^2) &= \sum_{i=0, \text{ even}}^{n-1} (-2\xi)^i B_{ni}(Q^2) - (-2\xi)^n C_{n0}(Q^2)|_{n \text{ even}}, \\
\int_{-1}^{+1} dx x^{n-1} \tilde{H}(x, \xi, Q^2) &= \sum_{i=0, \text{ even}}^{n-1} (-2\xi)^i \tilde{A}_{ni}(Q^2) + (-2\xi)^n \tilde{C}_{n0}(Q^2)|_{n \text{ even}},
\end{aligned} \tag{14}$$

where the unpolarized (polarized) generalized form factors (GFFs) $A_{ni}(Q^2)$, $B_{ni}(Q^2)$ and $C_{ni}(Q^2)$ ($\tilde{A}_{ni}(Q^2)$, and $\tilde{C}_{ni}(Q^2)$) in the ξ -expansion on the right-hand side are real functions. When $n = 1$ ($n = 2$), we get the Dirac and Pauli electromagnetic form factors $F_1(Q^2) = A_{10}(Q^2)$ and $F_2(Q^2) = B_{10}(Q^2)$ (GFFs $\{A, B\}_{20}(Q^2)$) and axial form factors $G_A(Q^2) = \tilde{A}_{10}(Q^2)$ (GFFs $\tilde{A}_{20}(Q^2)$). The LaMET-calculated GPDs can now compare with years of LQCD calculations using the OPE method.

Figure 8 shows the $n = 1$ moments of MSULat's x -dependent GPDs calculated at physical pion mass, along side with prior LQCD OPE calculations. To compare with other lattice results, the Sachs electric and magnetic form factors using $F_{1,2}$ as $G_E(Q^2) = F_1(Q^2) + q^2 F_2(Q^2)/(2M_N)^2$ and $G_M(Q^2) = F_1(Q^2) + F_2(Q^2)$ is plotted. The green band indicates results from x -dependent GPDs while the OPE calculated are shown in data points. One can see a nice agreement among the method and different LQCD calculations. Taking the $n = 2$ moment of MSULat's x -dependent GPD results with those obtained from Generalized form factor at/near the physical pion mass using OPE methods [127, 128]. We note that even with the same OPE approach by the same collaboration, the two data sets for A_{20} in the ETMC calculation exhibit some tension. This is an indication that the systematic uncertainties are more complicated for these GFFs. Given that the blue points correspond to finer lattice spacing, larger volume and larger $M_\pi L$, we expect that the blue points have suppressed systematic uncertainties. MSULat's moment result $A_{20}(Q^2)$ is in better agreement with those obtained using the OPE approach at small momentum transfer Q^2 , while $B_{20}(Q^2)$ is in better agreement with OPE approaches at large Q^2 . The comparison between the $N_f = 2$ ETMC data and $N_f = 2$ RQCD data reveals agreement for A_{20} and B_{20} . However, the RQCD data have a different slope than the ETMC data, which is attributed to the different analysis methods and systematic uncertainties. Both MSULat's results and ETMC's are done using a single ensemble; future studies to include other lattice artifacts, such as lattice-spacing dependence, are important to account for the difference in the results.

MSULat group further took the Fourier transform of the non-spin-flip Q^2 -dependent GPD $H(x, \xi = 0, Q^2)$ to calculate the impact-parameter-dependent distribution [140] $\int \frac{d\mathbf{q}}{(2\pi)^2} H(x, \xi = 0, t = -\mathbf{q}^2) e^{i\mathbf{q} \cdot \mathbf{b}}$ where b is the transverse distance from the center of momentum [123]. Figure 9 shows the first LQCD results of impact-parameter-dependent 2D distributions at $x = 0.3, 0.5$ and 0.7 . The impact-parameter-dependent distribution describes the probability density for a parton with momentum fraction x at distance b in the transverse plane, providing x -dependent nucleon tomography using LQCD for the first time. Similar tomography results for helicity GPD, $\tilde{H}(x, \xi = 0, Q^2)$ can be found in Ref. [124].

4 Conclusion and Outlook

There will be more progress in understanding hadron spectroscopy using lattice-QCD methods and expanding to states with two or more final hadrons. Many tools and techniques have been created to extract excited-state spectroscopy at heavy pion masses. As the pion masses get lighter, multiple-particle final states will be important to include to extract the correct spectroscopy. More and more collaborations have started to include two-hadron final states to extract decay width and properties; future work will continue to push for more complicated final states in the lattice calculations.

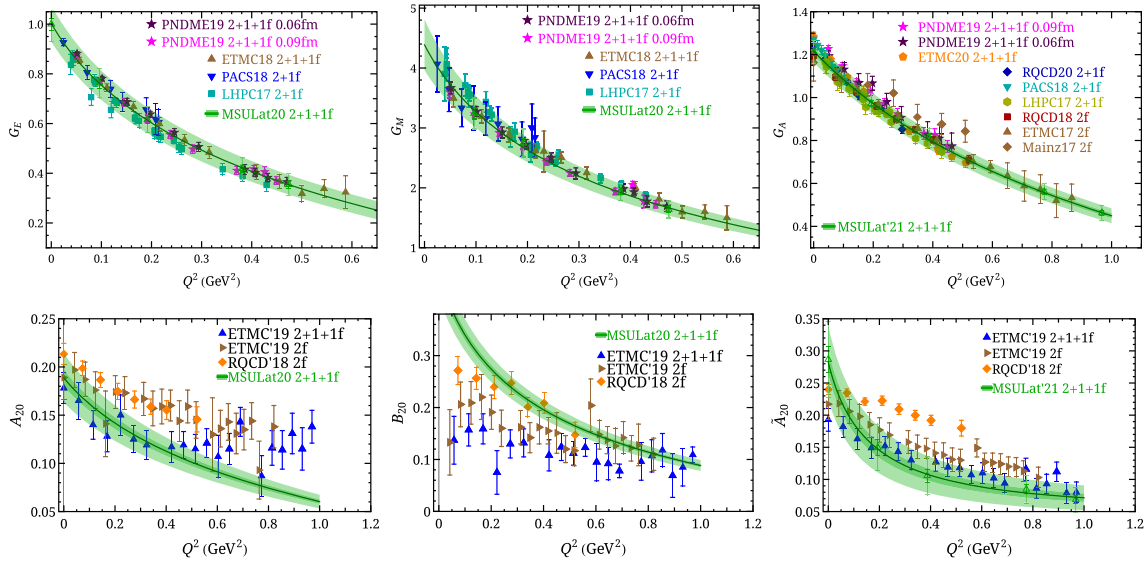


Fig. 8 (top) The nucleon isovector electric (left), magnetic (middle) and axial (right) form factor results obtained from x -dependent GPDs [123, 124] (labeled as green bands in the plots) as functions of transferred momentum Q^2 , and comparison with other lattice works calculated near physical pion mass [129–139]. (bottom) The unpolarized nucleon isovector GFFs $\{A, B\}_{20}(Q^2)$ $\tilde{A}_{20}(Q^2)$ obtained from x -dependent GPDs [123, 124] (labeled as green bands in the plots by taking $n = 2$ in Eq. 14, compared with other lattice results calculated near physical pion mass as functions of transfer momentum Q^2 [127, 128]

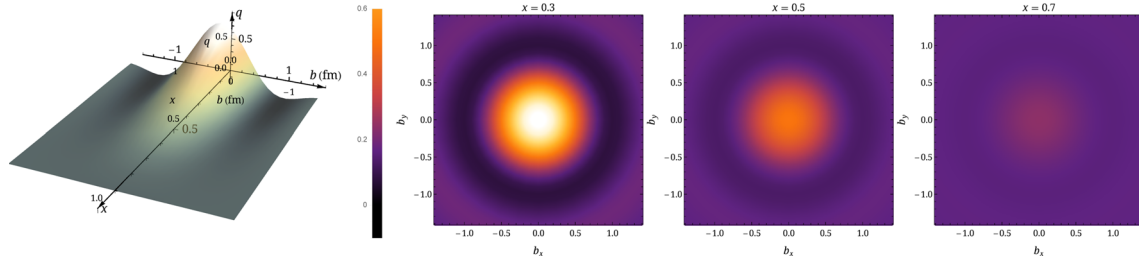


Fig. 9 (left) Nucleon tomography: three-dimensional impact parameter-dependent parton distribution as a function of x and b using lattice H at physical pion mass. (right) Two-dimensional impact-parameter-dependent isovector nucleon GPDs for $x = 0.3, 0.5$ and 0.7 from the lattice at physical pion mass [123]

This is an exciting era for using lattice QCD to study PDFs. The well-studied systematics of the traditional moment method allow LQCD to provide precision structure quantities directly at the physical pion masses with multiple lattice spacings. We are now also able to provide information on the Bjorken- x dependence of parton distributions, and they are widely studied with more than just the “quasi-PDF” method mentioned in this proceeding. Some lattice studies have begun to control systematics by using multiple lattice spacings and volumes; many such calculations are planned for near-future updates to improve the current calculations. We are also starting to address neglected disconnected contributions and taking a look into flavor-dependent quantities, but much work remains ahead. Stay tuned for more updates from lattice QCD in the near future.

Acknowledgements The work of HL is partially supported by the US National Science Foundation under grant PHY 1653405 and by the Research Corporation for Science Advancement through the Cottrell Scholar Award.

References

1. D. d’Enterria, S. Kluth, G. Zanderighi, et al., (2022). <https://doi.org/10.48550/arXiv.2203.08271> <https://doi.org/10.48550/arXiv.2203.08271>
2. C. Michael, Nucl. Phys. B **259**, 58 (1985). [https://doi.org/10.1016/0550-3213\(85\)90297-4](https://doi.org/10.1016/0550-3213(85)90297-4)
3. M. Luscher, U. Wolff, Nucl. Phys. B **339**, 222 (1990). [https://doi.org/10.1016/0550-3213\(90\)90540-T](https://doi.org/10.1016/0550-3213(90)90540-T)

4. S. Basak, R.G. Edwards, G.T. Fleming, U.M. Heller, C. Morningstar, D. Richards, I. Sato, S. Wallace, Phys. Rev. D **72**, 094506 (2005). <https://doi.org/10.1103/PhysRevD.72.094506>
5. S. Basak, R. Edwards, G.T. Fleming, U.M. Heller, C. Morningstar, D. Richards, I. Sato, S.J. Wallace, Phys. Rev. D **72**, 074501 (2005). <https://doi.org/10.1103/PhysRevD.72.074501>
6. A.C. Lichtl, *Quantum Operator Design for Lattice Baryon Spectroscopy*. Other thesis (2006). <https://doi.org/10.2172/917690>
7. S. Basak, R.G. Edwards, G.T. Fleming, J. Juge, A.C. Lichtl, C. Morningstar, D.G. Richards, I. Sato, S.J. Wallace (2006). <https://arxiv.org/pdf/hep-lat/0609052.pdf> <https://arxiv.org/pdf/hep-lat/0609052.pdf>
8. S. Basak, R.G. Edwards, G.T. Fleming, K.J. Juge, A. Lichtl, C. Morningstar, D.G. Richards, I. Sato, S.J. Wallace, Phys. Rev. D **76**, 074504 (2007). <https://doi.org/10.1103/PhysRevD.76.074504>
9. M. Peardon, J. Bulava, J. Foley, C. Morningstar, J. Dudek, R.G. Edwards, B. Joo, H.W. Lin, D.G. Richards, K.J. Juge, Phys. Rev. D **80**, 054506 (2009). <https://doi.org/10.1103/PhysRevD.80.054506>
10. C. Morningstar, A. Bell, C.Y. Chen, D. Lenkner, C.H. Wong, J. Bulava, J. Foley, K.J. Juge, M. Peardon, PoS, in **ICHEP2010** (2010), p. 369. <https://doi.org/10.22323/1.120.0369>
11. J. Bulava, J. Foley, K.J. Juge, C.J. Morningstar, M.J. Peardon, C.H. Wong, PoS, in **LATTICE2010** (2010), p. 110. <https://doi.org/10.22323/1.105.0110>
12. C. Morningstar, J. Bulava, J. Foley, K.J. Juge, D. Lenkner, M. Peardon, C.H. Wong, Phys. Rev. D **83**, 114505 (2011). <https://doi.org/10.1103/PhysRevD.83.114505>
13. M. Luscher, Commun. Math. Phys. **105**, 153 (1986). <https://doi.org/10.1007/BF01211097>
14. M. Luscher, Nucl. Phys. B **354**, 531 (1991). [https://doi.org/10.1016/0550-3213\(91\)90366-6](https://doi.org/10.1016/0550-3213(91)90366-6)
15. K. Rummukainen, S.A. Gottlieb, Nucl. Phys. B **450**, 397 (1995). [https://doi.org/10.1016/0550-3213\(95\)00313-H](https://doi.org/10.1016/0550-3213(95)00313-H)
16. X. Feng, X. Li, C. Liu, Phys. Rev. D **70**, 014505 (2004). <https://doi.org/10.1103/PhysRevD.70.014505>
17. S. He, X. Feng, C. Liu, JHEP **07**, 011 (2005). <https://doi.org/10.1088/1126-6708/2005/07/011>
18. P.F. Bedaque, Phys. Lett. B **593**, 82 (2004). <https://doi.org/10.1016/j.physletb.2004.04.045>
19. C. Liu, X. Feng, S. He, Int. J. Mod. Phys. A **21**, 847 (2006). <https://doi.org/10.1142/S0217751X06032150>
20. C.H. Kim, C.T. Sachrajda, S.R. Sharpe, Nucl. Phys. B **727**, 218 (2005). <https://doi.org/10.1016/j.nuclphysb.2005.08.029>
21. N.H. Christ, C. Kim, T. Yamazaki, Phys. Rev. D **72**, 114506 (2005). <https://doi.org/10.1103/PhysRevD.72.114506>
22. M. Lage, U.G. Meissner, A. Rusetsky, Phys. Lett. B **681**, 439 (2009). <https://doi.org/10.1016/j.physletb.2009.10.055>
23. V. Bernard, M. Lage, U.G. Meissner, A. Rusetsky, JHEP **01**, 019 (2011). [https://doi.org/10.1007/JHEP01\(2011\)019](https://doi.org/10.1007/JHEP01(2011)019)
24. Z. Fu, Phys. Rev. D **85**, 014506 (2012). <https://doi.org/10.1103/PhysRevD.85.014506>
25. L. Leskovec, S. Prelovsek, Phys. Rev. D **85**, 114507 (2012). <https://doi.org/10.1103/PhysRevD.85.114507>
26. R.A. Briceno, Z. Davoudi, Phys. Rev. D **88**(9), 094507 (2013). <https://doi.org/10.1103/PhysRevD.88.094507>
27. M.T. Hansen, S.R. Sharpe, Phys. Rev. D **86**, 016007 (2012). <https://doi.org/10.1103/PhysRevD.86.016007>
28. P. Guo, J. Dudek, R. Edwards, A.P. Szczepaniak, Phys. Rev. D **88**(1), 014501 (2013). <https://doi.org/10.1103/PhysRevD.88.014501>
29. N. Li, C. Liu, Phys. Rev. D **87**(1), 014502 (2013). <https://doi.org/10.1103/PhysRevD.87.014502>
30. R.A. Briceno, Z. Davoudi, T.C. Luu, M.J. Savage, Phys. Rev. D **89**(7), 074509 (2014). <https://doi.org/10.1103/PhysRevD.89.074509>
31. R.A. Briceno, Phys. Rev. D **89**(7), 074507 (2014). <https://doi.org/10.1103/PhysRevD.89.074507>
32. S. Aoki et al., Phys. Rev. D **76**, 094506 (2007). <https://doi.org/10.1103/PhysRevD.76.094506>
33. X. Feng, K. Jansen, D.B. Renner, Phys. Rev. D **83**, 094505 (2011). <https://doi.org/10.1103/PhysRevD.83.094505>
34. C.B. Lang, D. Mohler, S. Prelovsek, M. Vidmar, Phys. Rev. D **84**(5), 054503 (2011). <https://doi.org/10.1103/PhysRevD.84.054503> [Erratum: Phys. Rev. D **89**, 059903 (2014)]
35. S. Aoki et al., Phys. Rev. D **84**, 094505 (2011). <https://doi.org/10.1103/PhysRevD.84.094505>
36. J.J. Dudek, R.G. Edwards, C.E. Thomas, Phys. Rev. D **87**(3), 034505 (2013). <https://doi.org/10.1103/PhysRevD.87.034505> [Erratum: Phys. Rev. D **90**, 099902 (2014)]
37. C. Pelissier, A. Alexandru, Phys. Rev. D **87**(1), 014503 (2013). <https://doi.org/10.1103/PhysRevD.87.014503>
38. D.J. Wilson, R.A. Briceno, J.J. Dudek, R.G. Edwards, C.E. Thomas, Phys. Rev. D **92**(9), 094502 (2015). <https://doi.org/10.1103/PhysRevD.92.094502>
39. G.S. Bali, S. Collins, A. Cox, G. Donald, M. Göckeler, C.B. Lang, A. Schäfer, Phys. Rev. D **93**(5), 054509 (2016). <https://doi.org/10.1103/PhysRevD.93.054509>
40. J. Bulava, B. Fahy, B. Hörz, K.J. Juge, C. Morningstar, C.H. Wong, Nucl. Phys. B **910**, 842 (2016). <https://doi.org/10.1016/j.nuclphysb.2016.07.024>
41. D. Guo, A. Alexandru, R. Molina, M. Döring, Phys. Rev. D **94**(3), 034501 (2016). <https://doi.org/10.1103/PhysRevD.94.034501>
42. R.A. Briceno, J.J. Dudek, R.G. Edwards, D.J. Wilson, Phys. Rev. Lett. **118**(2), 022002 (2017). <https://doi.org/10.1103/PhysRevLett.118.022002>
43. D. Guo, A. Alexandru, R. Molina, M. Mai, M. Döring, Phys. Rev. D **98**(1), 014507 (2018). <https://doi.org/10.1103/PhysRevD.98.014507>
44. C.B. Lang, L. Leskovec, D. Mohler, S. Prelovsek, Phys. Rev. D **86**, 054508 (2012). <https://doi.org/10.1103/PhysRevD.86.054508>
45. Z. Fu, K. Fu, Phys. Rev. D **86**, 094507 (2012). <https://doi.org/10.1103/PhysRevD.86.094507>
46. S. Prelovsek, L. Leskovec, C.B. Lang, D. Mohler, Phys. Rev. D **88**(5), 054508 (2013). <https://doi.org/10.1103/PhysRevD.88.054508>
47. R. Brett, J. Bulava, J. Fallica, A. Hanlon, B. Hörz, C. Morningstar, Nucl. Phys. B **932**, 29 (2018). <https://doi.org/10.1016/j.nuclphysb.2018.05.008>
48. C.W. Andersen, J. Bulava, B. Hörz, C. Morningstar, Phys. Rev. D **97**(1), 014506 (2018). <https://doi.org/10.1103/PhysRevD.97.014506>

49. J.J. Dudek, R.G. Edwards, C.E. Thomas, D.J. Wilson, Phys. Rev. Lett. **113**(18), 182001 (2014). <https://doi.org/10.1103/PhysRevLett.113.182001>
50. D.J. Wilson, J.J. Dudek, R.G. Edwards, C.E. Thomas, Phys. Rev. D **91**(5), 054008 (2015). <https://doi.org/10.1103/PhysRevD.91.054008>
51. G. Moir, M. Peardon, S.M. Ryan, C.E. Thomas, D.J. Wilson, JHEP **10**, 011 (2016). [https://doi.org/10.1007/JHEP10\(2016\)011](https://doi.org/10.1007/JHEP10(2016)011)
52. J.J. Dudek, R.G. Edwards, D.J. Wilson, Phys. Rev. D **93**(9), 094506 (2016). <https://doi.org/10.1103/PhysRevD.93.094506>
53. R.A. Briceño, J.J. Dudek, R.G. Edwards, D.J. Wilson, Phys. Rev. D **97**(5), 054513 (2018). <https://doi.org/10.1103/PhysRevD.97.054513>
54. R.A. Briceño, J.J. Dudek, R.G. Edwards, C.J. Shultz, C.E. Thomas, D.J. Wilson, Phys. Rev. Lett. **115**, 242001 (2015). <https://doi.org/10.1103/PhysRevLett.115.242001>
55. R.A. Briceño, J.J. Dudek, R.G. Edwards, C.J. Shultz, C.E. Thomas, D.J. Wilson, Phys. Rev. D **93**(11), 114508 (2016). <https://doi.org/10.1103/PhysRevD.93.114508>
56. R.A. Briceño, J.J. Dudek, R.D. Young, Rev. Mod. Phys. **90**(2), 025001 (2018). <https://doi.org/10.1103/RevModPhys.90.025001>
57. M. Padmanath, PoS, in **LATTICE2018** (2018), p. 013. <https://doi.org/10.22323/1.334.0013>
58. W. Detmold, R.G. Edwards, J.J. Dudek, M. Engelhardt, H.W. Lin, S. Meinel, K. Orginos, P. Shanahan, Eur. Phys. J. A **55**(11), 193 (2019). <https://doi.org/10.1140/epja/i2019-12902-4>
59. J. Bulava, et al., in *2022 Snowmass Summer Study* (2022)
60. R. Gupta, Y.C. Jang, B. Yoon, H.W. Lin, V. Cirigliano, T. Bhattacharya, Phys. Rev. D **98**, 034503 (2018). <https://doi.org/10.1103/PhysRevD.98.034503>
61. H.W. Lin, J.W. Chen, X. Ji, L. Jin, R. Li, Y.S. Liu, Y.B. Yang, J.H. Zhang, Y. Zhao, Phys. Rev. Lett. **121**(24), 242003 (2018). <https://doi.org/10.1103/PhysRevLett.121.242003>
62. T. Bhattacharya, V. Cirigliano, S. Cohen, R. Gupta, H.W. Lin, B. Yoon, Phys. Rev. D **94**(5), 054508 (2016). <https://doi.org/10.1103/PhysRevD.94.054508>
63. T. Bhattacharya, V. Cirigliano, S. Cohen, R. Gupta, A. Joseph, H.W. Lin, B. Yoon, Phys. Rev. D **92**(9), 094511 (2015). <https://doi.org/10.1103/PhysRevD.92.094511>
64. J.R. Green, J.W. Negele, A.V. Pochinsky, S.N. Syritsyn, M. Engelhardt, S. Krieg, Phys. Rev. D **86**, 114509 (2012). <https://doi.org/10.1103/PhysRevD.86.114509>
65. Y. Aoki, T. Blum, H.W. Lin, S. Ohta, S. Sasaki, R. Tweedie, J. Zanotti, T. Yamazaki, Phys. Rev. D **82**, 014501 (2010). <https://doi.org/10.1103/PhysRevD.82.014501>
66. A. Abdel-Rehim et al., Phys. Rev. D **92**(11), 114513 (2015). <https://doi.org/10.1103/PhysRevD.92.114513>. [Erratum: Phys. Rev. D **93**, 039904 (2016)]
67. G.S. Bali, S. Collins, B. Glässle, M. Göckeler, J. Najjar, R.H. Rödl, A. Schäfer, R.W. Schiel, W. Söldner, A. Sternbeck, Phys. Rev. D **91**(5), 054501 (2015). <https://doi.org/10.1103/PhysRevD.91.054501>
68. T. Yamazaki, Y. Aoki, T. Blum, H.W. Lin, M.F. Lin, S. Ohta, S. Sasaki, R.J. Tweedie, J.M. Zanotti, Phys. Rev. Lett. **100**, 171602 (2008). <https://doi.org/10.1103/PhysRevLett.100.171602>
69. H.W. Lin, W. Melnitchouk, A. Prokudin, N. Sato, H. Shows, Phys. Rev. Lett. **120**(15), 152502 (2018). <https://doi.org/10.1103/PhysRevLett.120.152502>
70. H.W. Lin et al., Prog. Part. Nucl. Phys. **100**, 107 (2018). <https://doi.org/10.1016/j.pnnp.2018.01.007>
71. M. Constantinou et al., Prog. Part. Nucl. Phys. **121**, 103908 (2021). <https://doi.org/10.1016/j.pnnp.2021.103908>
72. X. Ji, Phys. Rev. Lett. **110**, 262002 (2013). <https://doi.org/10.1103/PhysRevLett.110.262002>
73. X. Ji, Sci. China Phys. Mech. Astron. **57**, 1407 (2014). <https://doi.org/10.1007/s11433-014-5492-3>
74. Y.Q. Ma, J.W. Qiu, Phys. Rev. Lett. **120**(2), 022003 (2018). <https://doi.org/10.1103/PhysRevLett.120.022003>
75. T. Izubuchi, X. Ji, L. Jin, I.W. Stewart, Y. Zhao, Phys. Rev. D **98**(5), 056004 (2018). <https://doi.org/10.1103/PhysRevD.98.056004>
76. Y.S. Liu, W. Wang, J. Xu, Q.A. Zhang, J.H. Zhang, S. Zhao, Y. Zhao, Phys. Rev. D **100**(3), 034006 (2019). <https://doi.org/10.1103/PhysRevD.100.034006>
77. H.W. Lin, J.W. Chen, S.D. Cohen, X. Ji, Phys. Rev. D **91**, 054510 (2015). <https://doi.org/10.1103/PhysRevD.91.054510>
78. X. Ji, Y.S. Liu, Y. Liu, J.H. Zhang, Y. Zhao, Rev. Mod. Phys. **93**(3), 035005 (2021). <https://doi.org/10.1103/RevModPhys.93.035005>
79. X. Ji (2020). <https://arxiv.org/pdf/2007.06613.pdf>
80. M. Constantinou et al., Prog. Part. Nucl. Phys. **121**, 103908 (2021). <https://doi.org/10.1016/j.pnnp.2021.103908>
81. H.W. Lin, J.W. Chen, R. Zhang (2020). <https://arxiv.org/pdf/2011.14971.pdf>
82. T.J. Hou et al., Phys. Rev. D **103**(1), 014013 (2021). <https://doi.org/10.1103/PhysRevD.103.014013>
83. R.D. Ball et al., Eur. Phys. J. C **77**(10), 663 (2017). <https://doi.org/10.1140/epjc/s10052-017-5199-5>
84. S. Alekhin, J. Blümlein, S. Moch, R. Placakyte, Phys. Rev. D **96**(1), 014011 (2017). <https://doi.org/10.1103/PhysRevD.96.014011>
85. A. Accardi, L.T. Brady, W. Melnitchouk, J.F. Owens, N. Sato, Phys. Rev. D **93**(11), 114017 (2016). <https://doi.org/10.1103/PhysRevD.93.114017>
86. C. Alexandrou, K. Cichy, M. Constantinou, K. Jansen, A. Scapellato, F. Steffens, Phys. Rev. Lett. **121**(11), 112001 (2018). <https://doi.org/10.1103/PhysRevLett.121.112001>
87. C. Alexandrou, K. Cichy, M. Constantinou, K. Jansen, A. Scapellato, F. Steffens, Phys. Rev. D **98**(9), 091503 (2018). <https://doi.org/10.1103/PhysRevD.98.091503>
88. Y.S. Liu, J.W. Chen, L. Jin, R. Li, H.W. Lin, Y.B. Yang, J.H. Zhang, Y. Zhao (2018). <https://doi.org/10.05043.pdf>
89. E.R. Nocera, R.D. Ball, S. Forte, G. Ridolfi, J. Rojo, Nucl. Phys. B **887**, 276 (2014). <https://doi.org/10.1016/j.nuclphysb.2014.08.008>
90. J.J. Ethier, N. Sato, W. Melnitchouk, Phys. Rev. Lett. **119**(13), 132001 (2017). <https://doi.org/10.1103/PhysRevLett.119.132001>

91. Y. Lu, L. Chang, K. Raya, C.D. Roberts, J. Rodríguez-Quintero, Phys. Lett. B **830**, 137130 (2022). <https://doi.org/10.1016/j.physletb.2022.137130>
92. C. Alexandrou, K. Cichy, M. Constantinou, K. Hadjiyiannakou, K. Jansen, A. Scapellato, F. Steffens, Phys. Rev. D **99**(11), 114504 (2019). <https://doi.org/10.1103/PhysRevD.99.114504>
93. D. de Florian, R. Sassot, M. Stratmann, W. Vogelsang, Phys. Rev. D **80**, 034030 (2009). <https://doi.org/10.1103/PhysRevD.80.034030>
94. J. Benel, A. Courtoy, R. Ferro-Hernandez, Eur. Phys. J. C **80**(5), 465 (2020). <https://doi.org/10.1140/epjc/s10052-020-8039-y>
95. M. Radici, A. Bacchetta, Phys. Rev. Lett. **120**(19), 192001 (2018). <https://doi.org/10.1103/PhysRevLett.120.192001>
96. R. Zhang, H.W. Lin, B. Yoon, Phys. Rev. D **104**(9), 094511 (2021). <https://doi.org/10.1103/PhysRevD.104.094511>
97. J.H. Zhang, J.W. Chen, L. Jin, H.W. Lin, A. Schäfer, Y. Zhao, Phys. Rev. D **100**(3), 034505 (2019). <https://doi.org/10.1103/PhysRevD.100.034505>
98. H.W. Lin, J.W. Chen, Z. Fan, J.H. Zhang, R. Zhang, Phys. Rev. D **103**(1), 014516 (2021). <https://doi.org/10.1103/PhysRevD.103.014516>
99. C. Chen, L. Chang, C.D. Roberts, S. Wan, H.S. Zong, Phys. Rev. D **93**(7), 074021 (2016). <https://doi.org/10.1103/PhysRevD.93.074021>
100. G.R. Farrar, D.R. Jackson, Phys. Rev. Lett. **35**, 1416 (1975). <https://doi.org/10.1103/PhysRevLett.35.1416>
101. E.L. Berger, S.J. Brodsky, Phys. Rev. Lett. **42**, 940 (1979). <https://doi.org/10.1103/PhysRevLett.42.940>
102. R.S. Sufian, C. Egerer, J. Karpie, R.G. Edwards, B. Joó, Y.Q. Ma, K. Orginos, J.W. Qiu, D.G. Richards, Phys. Rev. D **102**(5), 054508 (2020). <https://doi.org/10.1103/PhysRevD.102.054508>
103. R.S. Sufian, J. Karpie, C. Egerer, K. Orginos, J.W. Qiu, D.G. Richards, Phys. Rev. D **99**(7), 074507 (2019). <https://doi.org/10.1103/PhysRevD.99.074507>
104. T. Nguyen, A. Bashir, C.D. Roberts, P.C. Tandy, Phys. Rev. C **83**, 062201 (2011). <https://doi.org/10.1103/PhysRevC.83.062201>
105. J. Lan, C. Mondal, S. Jia, X. Zhao, J.P. Vary, Phys. Rev. Lett. **122**(17), 172001 (2019). <https://doi.org/10.1103/PhysRevLett.122.172001>
106. Z. Fan, H.W. Lin, Phys. Lett. B **823**, 136778 (2021). <https://doi.org/10.1016/j.physletb.2021.136778>
107. Z. Fan, H.W. Lin, in *38th International Symposium on Lattice Field Theory* (2021)
108. Z.Y. Fan, Y.B. Yang, A. Anthony, H.W. Lin, K.F. Liu, Phys. Rev. Lett. **121**(24), 242001 (2018). <https://doi.org/10.1103/PhysRevLett.121.242001>
109. J. Butterworth et al., J. Phys. G **43**, 023001 (2016). <https://doi.org/10.1088/0954-3889/43/2/023001>
110. S. Dulat, T.J. Hou, J. Gao, M. Guzzi, J. Huston, P. Nadolsky, J. Pumplin, C. Schmidt, D. Stump, C.P. Yuan, Phys. Rev. D **93**(3), 033006 (2016). <https://doi.org/10.1103/PhysRevD.93.033006>
111. I. Balitsky, W. Morris, A. Radyushkin, Phys. Lett. B **808**, 135621 (2020). <https://doi.org/10.1016/j.physletb.2020.135621>
112. W. Wang, J.H. Zhang, S. Zhao, R. Zhu, Phys. Rev. D **100**(7), 074509 (2019). <https://doi.org/10.1103/PhysRevD.100.074509>
113. J.H. Zhang, X. Ji, A. Schäfer, W. Wang, S. Zhao, Phys. Rev. Lett. **122**(14), 142001 (2019). <https://doi.org/10.1103/PhysRevLett.122.142001>
114. Z. Fan, R. Zhang, H.W. Lin, Int. J. Mod. Phys. A **36**(13), 2150080 (2021). <https://doi.org/10.1142/S0217751X21500809>
115. Z.F. Cui, M. Ding, F. Gao, K. Raya, D. Binosi, L. Chang, C.D. Roberts, J. Rodríguez-Quintero, S.M. Schmidt, Eur. Phys. J. C **80**(11), 1064 (2020). <https://doi.org/10.1140/epjc/s10052-020-08578-4>
116. P.C. Barry, N. Sato, W. Melnitchouk, C.R. Ji, Phys. Rev. Lett. **121**(15), 152001 (2018). <https://doi.org/10.1103/PhysRevLett.121.152001>
117. N.Y. Cao, P.C. Barry, N. Sato, W. Melnitchouk (2021). <https://arxiv.org/pdf/2103.02159.pdf>
118. I. Novikov et al., Phys. Rev. D **102**(1), 014040 (2020). <https://doi.org/10.1103/PhysRevD.102.014040>
119. X.D. Ji, Phys. Rev. Lett. **78**, 610 (1997). <https://doi.org/10.1103/PhysRevLett.78.610>
120. X.D. Ji, Phys. Rev. D **55**, 7114 (1997). <https://doi.org/10.1103/PhysRevD.55.7114>
121. J.W. Chen, H.W. Lin, J.H. Zhang, Nucl. Phys. B **952**, 114940 (2020). <https://doi.org/10.1016/j.nuclphysb.2020.114940>
122. C. Alexandrou, K. Cichy, M. Constantinou, K. Hadjiyiannakou, K. Jansen, A. Scapellato, F. Steffens, Phys. Rev. Lett. **125**(26), 262001 (2020). <https://doi.org/10.1103/PhysRevLett.125.262001>
123. H.W. Lin, Phys. Rev. Lett. **127**(18), 182001 (2021). <https://doi.org/10.1103/PhysRevLett.127.182001>
124. H.W. Lin, Phys. Lett. B **824**, 136821 (2022). <https://doi.org/10.1016/j.physletb.2021.136821>
125. X.D. Ji, J. Phys. G **24**, 1181 (1998). <https://doi.org/10.1088/0954-3889/24/7/002>
126. P. Hagler, Phys. Rep. **490**, 49 (2010). <https://doi.org/10.1016/j.physrep.2009.12.008>
127. C. Alexandrou et al., Phys. Rev. D **101**(3), 034519 (2020). <https://doi.org/10.1103/PhysRevD.101.034519>
128. G.S. Bali, S. Collins, M. Göckeler, R. Rödl, A. Schäfer, A. Sternbeck, Phys. Rev. D **100**(1), 014507 (2019). <https://doi.org/10.1103/PhysRevD.100.014507>
129. J.R. Green, J.W. Negele, A.V. Pochinsky, S.N. Syritsyn, M. Engelhardt, S. Krieg, Phys. Rev. D **90**, 074507 (2014). <https://doi.org/10.1103/PhysRevD.90.074507>
130. R. Gupta, Y.C. Jang, H.W. Lin, B. Yoon, T. Bhattacharya, Phys. Rev. D **96**(11), 114503 (2017). <https://doi.org/10.1103/PhysRevD.96.114503>
131. N. Hasan, J. Green, S. Meinel, M. Engelhardt, S. Krieg, J. Negele, A. Pochinsky, S. Syritsyn, Phys. Rev. D **97**(3), 034504 (2018). <https://doi.org/10.1103/PhysRevD.97.034504>
132. S. Capitani, M. Della Morte, D. Djukanovic, G.M. von Hippel, J. Hua, B. Jäger, P.M. Junnarkar, H.B. Meyer, T.D. Rae, H. Wittig, Int. J. Mod. Phys. A **34**(02), 1950009 (2019). <https://doi.org/10.1142/S0217751X1950009X>
133. C. Alexandrou, M. Constantinou, K. Hadjiyiannakou, K. Jansen, C. Kallidonis, G. Koutsou, A. Vaquero Aviles-Casco, Phys. Rev. D **96**(5), 054507 (2017). <https://doi.org/10.1103/PhysRevD.96.054507>
134. G.S. Bali, S. Collins, M. Gruber, A. Schäfer, P. Wein, T. Wurm, Phys. Lett. B **789**, 666 (2019). <https://doi.org/10.1016/j.physletb.2018.12.053>

135. C. Alexandrou, S. Bacchio, M. Constantinou, J. Finkenrath, K. Hadjiyiannakou, K. Jansen, G. Koutsou, A. Vaquero Aviles-Casco, Phys. Rev. D **100**(1), 014509 (2019). <https://doi.org/10.1103/PhysRevD.100.014509>
136. Y.C. Jang, T. Bhattacharya, R. Gupta, H.W. Lin, B. Yoon, PoS, in **LATTICE2018** (2018), 123. <https://doi.org/10.22323/1.334.0123>
137. E. Shintani, K.I. Ishikawa, Y. Kuramashi, S. Sasaki, T. Yamazaki, Phys. Rev. D **99**(1), 014510 (2019). <https://doi.org/10.1103/PhysRevD.99.014510>. [Erratum: Phys.Rev.D 102, 019902 (2020)]
138. G.S. Bali, L. Barca, S. Collins, M. Gruber, M. Löffler, A. Schäfer, W. Söldner, P. Wein, S. Weishäupl, T. Wurm, JHEP **05**, 126 (2020). [https://doi.org/10.1007/JHEP05\(2020\)126](https://doi.org/10.1007/JHEP05(2020)126)
139. C. Alexandrou et al., Phys. Rev. D **103**(3), 034509 (2021). <https://doi.org/10.1103/PhysRevD.103.034509>
140. M. Burkardt, Int. J. Mod. Phys. A **18**, 173 (2003). <https://doi.org/10.1142/S0217751X03012370>

Publisher's Note Springer Nature remains neutral with regard to jurisdictional claims in published maps and institutional affiliations.

Springer Nature or its licensor holds exclusive rights to this article under a publishing agreement with the author(s) or other rightsholder(s); author self-archiving of the accepted manuscript version of this article is solely governed by the terms of such publishing agreement and applicable law.